

Large aperture adaptive doublet polymer lens for imaging applications

Freddie Santiago,^{1,*} Brett Bagwell,¹ Ty Martinez,² Sergio Restaino,² and Sanjay Krishna³

¹Sandia National Laboratories, Albuquerque, New Mexico 87123, USA

²U.S. Naval Research Laboratory, Code 7216, Washington DC 20375, USA

³Center for High Technology Materials, University of New Mexico, Albuquerque, New Mexico 87131, USA

*Corresponding author: fsantia@sandia.gov

Received May 16, 2014; accepted June 26, 2014;
posted June 30, 2014 (Doc. ID 212185); published July 28, 2014

We report a full design process—finite element modeling, fabrication, and characterization—of adaptive doublet polymer lenses. A first-order model was developed and used to design fluidic doublets, analogous to their glass counterparts. Two constant-volume fluidic chambers were enclosed by three flexible membranes, resulting in a variable focal length doublet with a clear aperture of 19.0 mm. Chromatic focal shift was then used to compare numerical modeling to experimentally measured results over a positive focal length range of 55–200 mm ($f/2.89$ to $f/10.5$). © 2014 Optical Society of America

OCIS codes: (220.0220) Optical design and fabrication; (220.1080) Active or adaptive optics; (220.3630) Lenses; (220.4610) Optical fabrication; (250.0250) Optoelectronics; (250.2080) Polymer active devices.

<http://dx.doi.org/10.1364/JOSAA.31.001842>

1. INTRODUCTION

Variable focal length or adaptive lenses have been proposed since the 1800s, with the first patent awarded in 1866 [1]. Over the past 10 years, there has been a resurgence of interest in this type of lens, initially with clear apertures of 5 mm or less, and based on actuation techniques, such as electrowetting, variable fluid volume, and mechanical deformation of a flexible surface [2–4]. Commercial entities such as Holochip and Optotune have subsequently developed larger adaptive lenses, on the order of 10 mm (actuated) and as large as 20 mm (manual) in diameter.

In the noncommercial arena, efforts by DARPA, the Naval Research Labs (NRL) [5], and Sandia National Labs (SNL) continue to push the threshold of these devices for military applications with an emphasis on larger clear aperture, robust actuation modalities, and superior wavefront quality ($<\lambda/2$). SNL is currently the pioneer in building and demonstrating variable magnification (zoom) systems, based on these devices. By replacing moving glass lenses with two or more variable focal length devices, low size, weight, and power (SWaP)–high-speed-optical zoom has been demonstrated [6–8].

In this context, there have been efforts to move beyond mere singlet lenses, containing only one or two flexible surfaces and single fluid. In one demonstrated configuration, using the electrowetting technique, the immiscible property of two incompatible fluids allowed for two separate fluid volumes, but was inherently aperture limited. A second proposed configuration enclosed two fluids between rigid optical windows, with an intermediate flexible membrane as the only variable, resulting in a low dynamic range due to the limited difference in refractive index across the variable surface. The third effort that we are aware of used two flexible membranes and multiple chambers, but required variable fluid

volume control in each chamber [9]. While the latter gives a large dynamic range, it creates practical problems (repeatability and reliability) from an implementation perspective [10–12]. All of these configurations present challenges for military applications, namely small aperture sizes, low dynamic range, and impractical actuation modalities.

We present a large aperture (19 mm), constant-volume, variable focal length doublet, where two optical fluids are enclosed and separated by three flexible polymer membranes. By applying pressure to the two outer membranes, we deform all three membranes, changing the radius of curvature (ROC). For this type of configuration, the behavior of the lens is determined not only by the fluid properties, but also by the membrane's mechanical properties, specifically the relative in-plane tension of each surface generated during the fabrication process.

We developed a first-order model that allowed us to go from an optical design to fabricating the adaptive doublet polymer lenses (ADPLs). This model required understanding the relationship between the pressure inside the lens, the volume enclosed in the lens hemisphere, and the in-plane tension of the membrane. Results from two doublets fabricated via this process are presented.

2. ADAPTIVE POLYMER LENS FABRICATION AND CONFIGURATION

SNL and NRL have developed a process that encompasses finite element modeling, polymer membrane research, development, and fabrication techniques in order to produce the best optical quality adaptive lens possible. Gravity-induced coma has been minimized by controlling the mechanical properties of the membrane, and thermally induced ROC and index changes are controlled by active athermalization [13].



Fig. 1. (Left) ADPL focusing on a business card. (Right) Side view of the ADPL showing support rings.

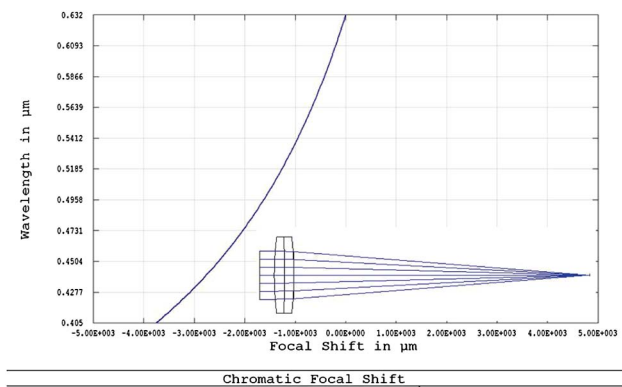
Figure 1 shows an ADPL. The lens is composed of rings that act as both the support structure and clear aperture boundary condition for the polydimethylsiloxane (PDMS) membranes. Because of our process, these rings can be made of almost any material. Glass, aluminum, titanium, and silicon carbide have been used.

Once the lens is made, it is inserted in the piezoelectric actuation mechanism that axially compresses the membrane, resulting in deformation. The actuator has a positional resolution of ≈ 40 nm, and no power is consumed once the desired ROC is achieved. Figure 8 shows a cross-sectional representation of an actuated ADPL.

In order to produce an ADPL with achromatic characteristics, fluids with crown and flint-like properties were selected for their index (n) and Abbe number (V). For the crown fluid $n_1 = 1.44$ and $V_1 = 62.2$, and for the flint $n_2 = 1.58$ and $V_2 = 29.0$. Zemax was used to design an ADPL using these fluids. Figure 2 shows an example of the ray-tracing sketch of the doublet, as well as the chromatic focal shift (at one focal length).

3. FROM DESIGN TO FABRICATION

In order to move from the optical design to fabrication, an understanding of the relationship between the pressure inside the lens, the volume of the encapsulated hemisphere, and the resultant ROCs needs to be established.



Maximum Focal Shift Range: 3757.5674 μm
 Diffraction Limited Range: 263.855 μm

Fig. 2. Chromatic focal shift plot for a designed ADPL and ray-tracing diagram.

A. Model: Linear Approximation

A finite element model (FEM) was developed to obtain the relationship between the pressure and volume of the spherical cap (V_{cap}) as a function of the membrane thickness. Using this relationship, the ROC can be determined analytically from the volume within the spherical cap. This relationship allows us to relate fabrication variables (thickness) to optical design parameters (ROC). The relationship between ROC and V_{cap} can be seen in Fig. 3, and is inversely proportional to ROC:

$$V_{\text{cap}} = \gamma \cdot \frac{1}{\text{ROC}}, \quad (1)$$

where γ is a proportionality factor.

We define the “thickness ratio” as

$$T_r = \frac{T_i}{T_f}, \quad (2)$$

where T_i is the initial thickness and T_f is the final thickness of the membrane once the in-plane stress has been applied. A uniform thin membrane was modeled in the FEM. Boundary conditions were established at the appropriate radii, and a pressure differential was created across the membrane for a given T_r . Figure 4 shows results from the FEM as well as a linear fit for three distinct T_r .

To determine the validity of these results, an experiment was designed to mimic the conditions of the FEM. The fixture shown in Fig. 5 was fabricated to encapsulate a membrane with a given T_r . A controlled pressure differential was applied to the membrane, and V_{cap} and ROC were measured *in situ*

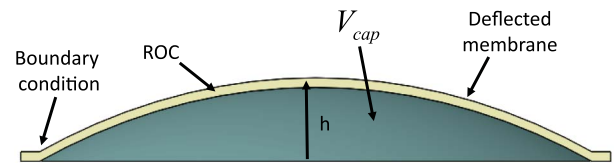


Fig. 3. Conceptual drawing showing the relationship between ROC and V_{cap} .

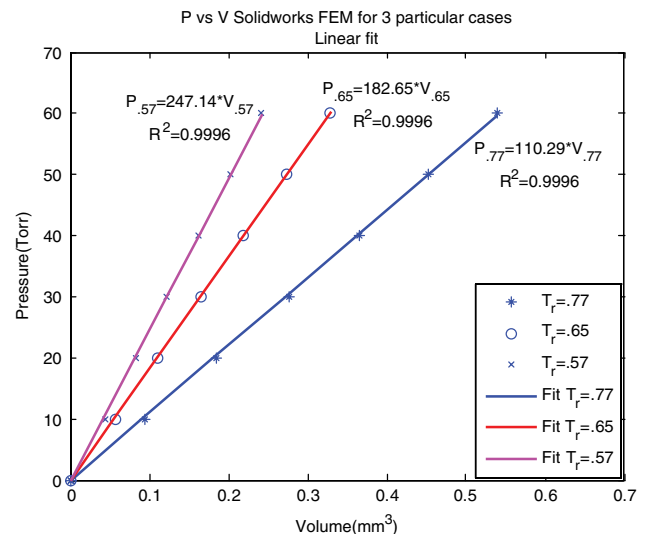


Fig. 4. Pressure versus volume results obtained from FEM and their respective linear fits.

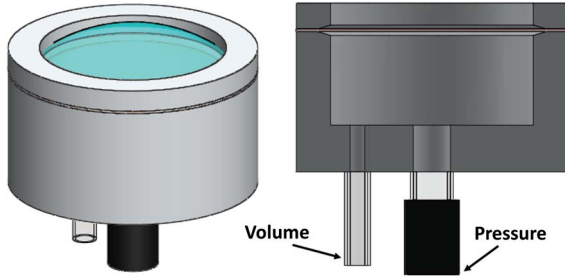


Fig. 5. Fixture used to measure pressure versus volume and ROC, as a function of T_r . The black port connects to a pressure gauge and measures the pressure inside the lens, and the clear port controls the volume and allows us to change the ROC.

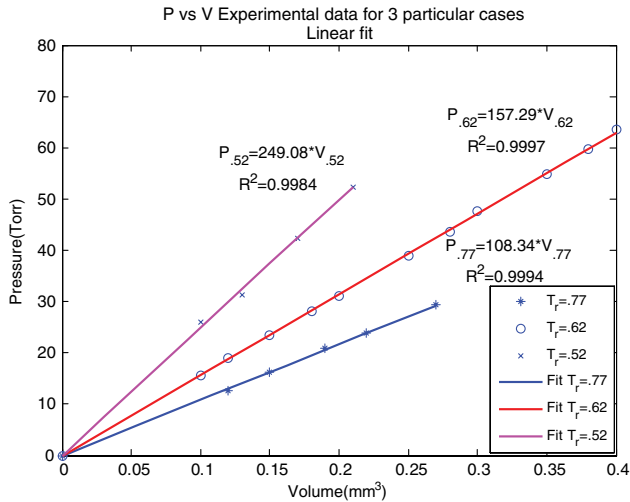


Fig. 6. Pressure versus volume results obtained from experimental results and their respective linear fits.

with a Zygo interferometer. Figure 6 shows the experimental results obtained for T_r , similar to that used in the FEM, as well as the fits obtained.

Figure 7 shows a plot of the FEM and the experimental data for $T_r = 0.76$. The high degree of concurrence between the model and measured data validated our first-order approach.

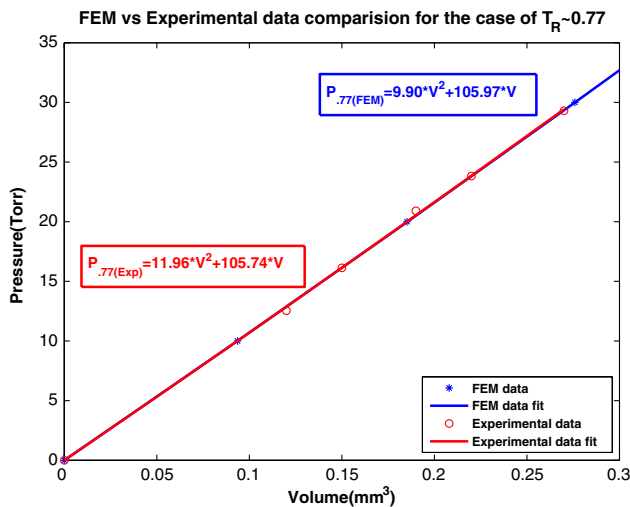


Fig. 7. Comparison between the FEM and experimental results for a thickness ratio of $T_r = 0.77$.

The experimental results confirmed a linear relationship between the change in pressure and the spherical cap:

$$\Delta P = m(T_r) * V_{cap}, \tag{3}$$

where m is a function of T_r . The relationship between m and T_r was obtained empirically from the slopes of each of the T_r and is of the form

$$m(T_r) = \alpha * T_r + \beta, \tag{4}$$

where α and β are empirically calculated constants and are dependent on the membrane's mechanical properties. For this case, the material is PDMS and they are equal to -499.48 and 484.22 , respectively.

By knowing T_r and the desired ROC, m can be calculated and the relationship between pressure and volume for a membrane of a particular thickness can be determined. In order to model a multiple flexible membrane lens, we need to apply a constant-volume condition, and express the differential in pressure across the membranes by

$$\Delta P_T = \sum_{n=1}^M \Delta P_n = \sum_{n=1}^M m_n * V_{cap_n} = 0, \tag{5}$$

where M is the total number of membranes and ΔP_n represents the pressure differential at each boundary. Figure 8 shows a cross-sectional schematic of a three-membrane lens.

From the ADPL prescription we obtain three ROCs and their associated V_{cap} . We then pick two thickness (ratios), which dictates their $m(T_r)$. Using Eq. (5) we solve for the remaining thickness ratio slope, $m(T_r)$. From $m(T_r)$, the remaining T_r can be determined from Eq. (4). Figure 9 illustrates a flow diagram of the design process.

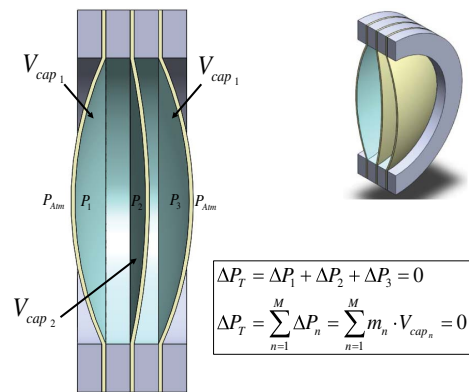


Fig. 8. Cross-sectional representation of an ADPL and pressure, volume, and thickness ratio relationship.

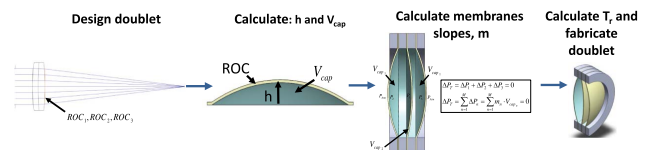


Fig. 9. Optical design to fabrication process for an ADPL.

4. OPTICAL SETUP AND EXPERIMENTAL RESULTS

A. ROC and Back Focal Length Determination

Once the doublet is fabricated, the outer ROCs (ROC₁ and ROC₂) of the ADPL are measured using a Zygo phase shift optical interferometer. The back focal distance (BFD) is measured using the testbed described in the next paragraph. Zemax was then used to determine ROC₂. Figure 10 graphically depicts the inner and outer radii of curvature, through the full dynamic range, of each of the fabricated ADPLs.

An optical benchtop setup was designed in which three lasers, of wavelengths 632, 532, and 405 nm, were expanded to fully illuminate the 19 mm clear aperture of the ADPL. A charge-coupled device (CCD) was placed on an optical translation stage with a micrometer, and one beam at a time was used to find the best focus. Once the best focus was identified, the position was recorded. The process was then repeated for the other two wavelengths, and the back focal length was measured as well. The APDL was then driven to another ROC, and the process was repeated. Figure 11 shows the optical setup.

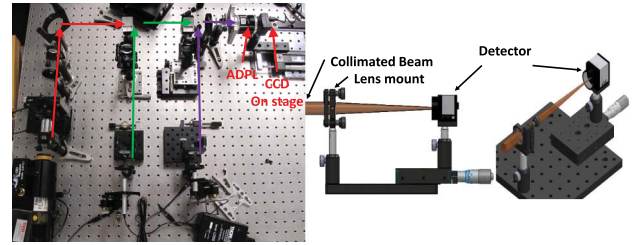


Fig. 11. Optical setup with three collimated beams at the wavelengths of interest, 632, 532, and 405 nm.

Table 1. Actuated ADPL Focal Shift Results for Two Achromatic Doublets Obtained from Measurements and Zemax Calculations with Their Respective Effective Focal Lengths (EFFLs)^a

EFFL	B-R			G-R		
	Measured	Zemax	Δ	Measured	Zemax	Δ
Doublet No. 1						
105.78	3.90	3.77	0.13	1.5	1.10	0.40
67.22	2.79	3.7	0.91	0.71	1.03	0.32
69.33	3.20	3.94	0.74	1.09	1.09	0
57.6	2.81	3.10	0.29	0.23	0.86	0.63
Doublet No. 2						
198.21	8.55	6.91	1.64	0.27	1.98	1.71
103.14	6.2	3.21	2.99	1.17	0.97	0.20
77.78	4.47	2.30	2.17	1.24	0.70	0.54
58.14	2.84	3.54	0.7	0.81	0.98	0.17
46.45	2.46	3.22	0.76	0.76	0.88	0.12

^aB-R refers to blue and red (405 and 632 nm), and G-R to green and red (532 and 632 nm). All values are in millimeters.

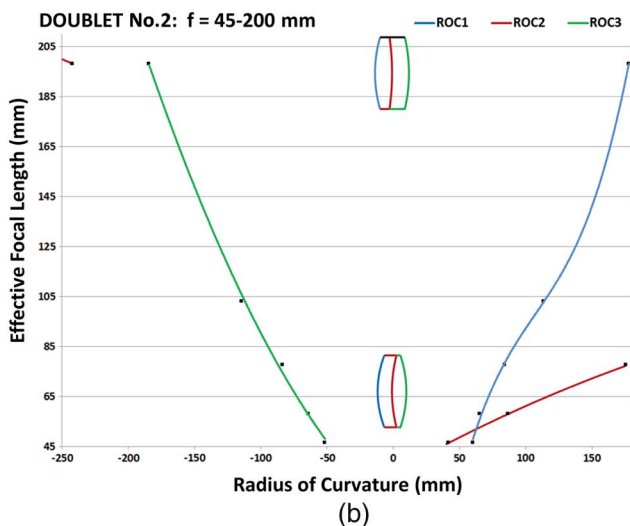
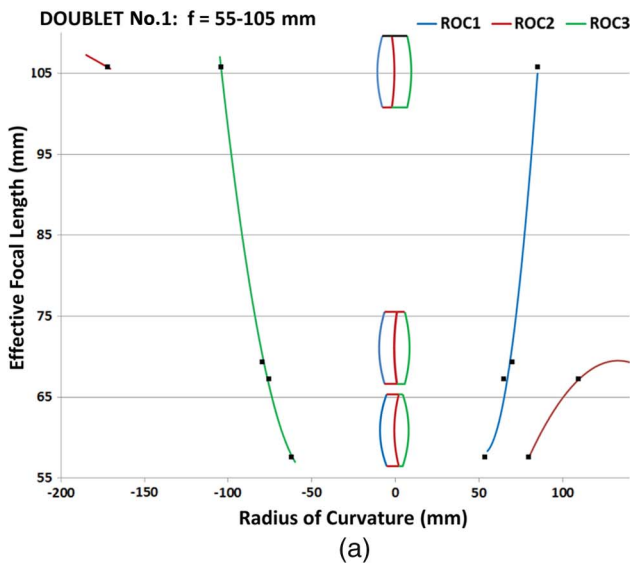


Fig. 10. Graphical representation of the measured prescription of ADPLs 1 and 2.

B. Chromatic Focal Shift Results

Table 1 shows the experimental and theoretical results for the two fabricated ADPLs.

The average focal shift measured on the ADPL was 4.13 mm for B-R and 0.87 mm for the G-R band. For both doublets, the calculated and measured G-R shifts are in better agreement than the B-R shifts.

5. CONCLUSIONS

We have demonstrated a first-order model that allows a three-surface, two-chamber, constant-volume, variable focal length lens to be fabricated. Via design optimization and characterization, we demonstrated that achromatization was achievable through the full dynamic range of the lens.

ACKNOWLEDGMENTS

Sandia National Laboratories is a multi-program laboratory managed and operated by Sandia Corporation, a wholly owned subsidiary of Lockheed Martin Corporation, for the U.S. Department of Energy's National Nuclear Security Administration under contract DE-AC04-94AL85000. SAND Number: 2014-3846 J.

REFERENCES

1. D. A. Woodward, "Improvement in fluid lenses," Letters Patent 60,109 (November 27, 1866).
2. B. Berge and J. Peseux, "Variable focal lens controlled by an external voltage: an application of electro-wetting," Eur. Phys. J. E **3**, 159–163 (2000).

3. S. Kuiper and B. H. W. Hendriks, "Variable-focus liquid lens for miniature cameras," *Appl. Phys. Lett.* **85**, 1128–1130 (2004).
4. H. Ren and S. Wu, *Introduction to Adaptive Lens* (Wiley, 2012).
5. G. Beadie, M. L. Sandrock, M. J. Wiggins, R. S. Lepkowitz, J. S. Shirk, M. Ponting, Y. Yang, T. Kazmierczak, A. Hiltner, and E. Baer, "Tunable polymer lens," *Opt. Express* **16**, 11847–11857 (2008).
6. B. E. Bagwell and F. Santiago, "RD100: RAZAR adaptive zoom rifle scope," RD100 (2014).
7. D. V. Wick, "Active optical zoom system," U.S. patent 6,977,777 (December 20, 2005).
8. D. V. Wick, T. Martinez, D. M. Payne, W. C. Sweatt, and S. R. Restaino, "Active optical zoom system," *Proc. SPIE* **5798**, 151–157 (2005).
9. P. Waibel, D. Mader, P. Liebetraut, H. Zappe, and A. Seifert, "Chromatic aberration control for tunable all-silicone membrane microlenses," *Opt. Express* **19**, 18584–18592 (2011).
10. A. Miks and J. Novak, "Analysis of two-element zoom systems based on variable power lenses," *Opt. Express* **18**, 6797–6810 (2010).
11. A. Miks and J. Novak, "Analysis of three-element zoom lens based on refractive variable-focus lenses," *Opt. Express* **19**, 23989–23996 (2011).
12. S. Reichelt and H. Zappe, "Design of spherically corrected, achromatic variable-focus liquid lenses," *Opt. Express* **15**, 14146–14154 (2007).
13. M. S. Baker, B. J. Anderson, G. Soehnel, B. Bagwell, and F. Santiago, "Polymer adaptive lens athermalization," Sandia Report SAND10 (Sandia National Laboratories, 2011).